Research Article | Vol. 25, No. 12 | 12 Jun 2017 | OPTICS EXPRESS 13760
Optics EXPRESS

Self-assembled flat-faceted nanoparticles chains as a highly-tunable platform for plasmon-enhanced spectroscopy in the infrared

GARIKOITZ AGUIRREGABIRIA,[1] JAVIER AIZPURUA,[1,2] AND RUBEN ESTEBAN[2,3,*]

[1]*Centro de Física de Materiales, Centro Mixto CSIC-UPV/EHU, 20018 Donostia-San Sebastián, Spain*
[2]*Donostia International Physics Center (DIPC), 20018 Donostia-San Sebastián, Spain*
[3]*IKERBASQUE, Basque Foundation for Science, 48013 Bilbao, Spain*
[*]*ruben_esteban@ehu.eus*

Abstract: Self-assembly fabrication methods can produce aggregates of metallic nanoparticles separated by nanometer distances which act as versatile platforms for field-enhanced spectroscopy due to the strong fields induced at the interparticle gaps. In this letter we show the advantages of using particles with large flat facets at the gap as the building elements of the aggregates. For this purpose, we analyze theoretically the plasmonic response of chains of metallic particles of increasing length. These chains may be a direct product of the chemical synthesis and can be seen as the key structural unit behind the plasmonic response of two and three dimensional self-assembled aggregates. The longitudinal chain plasmon that dominates the optical response redshifts following an exponential dependence on the number of particles in the chain for all facets studied, with a saturation wavelength and a characteristic decay length depending linearly on the diameter of the facet. According to our calculations, for small Au particles of 50 nm size separated by a 1 nanometer gap, the saturation wavelength for the largest facets considered correspond to a wavelength shift of ≈ 1200 nm with respect to the single particle resonance, compared to shifts of only ≈ 200 nm for the equivalent configuration of perfectly spherical particles. The corresponding decay lengths are 11.8 particles for the faceted nanoparticles and 3.5 particles for the spherical ones. Thus, large flat facets lead to an excellent tunability of the longitudinal chain plasmon, covering the whole biological window and beyond. Furthermore, the maximum near-field at the gap is only moderately weaker for faceted gaps than for spherical particles, while the region of strong local field enhancement extends over a considerably larger volume, allowing to accommodate more target molecules. Our results indicate that flat facets introduce significant advantages for spectroscopic and sensing applications using self-assembled aggregates.

OCIS codes: (250.5403) Plasmonics, (220.0220) Optical design and fabrication, (300.0300) Spectroscopy, (160.1245) Artificially engineered materials, (160.4236) Nanomaterials, (160.4760) Optical properties.

References and links

1. M. Pelton, J. Aizpurua, and G. Bryant, "Metal-nanoparticle plasmonics," Laser Photon. Rev. **2**, 136–159 (2008).
2. R. Vogelgesang and A. Dmitriev, "Real-space imaging of nanoplasmonic resonances," Analyst **135**, 1175–1181 (2010).
3. P. Mühlschlegel, H.-J. Eisler, O. Martin, B. Hecht, and D. Pohl, "Resonant optical antennas," Science **308**, 1607–1609 (2005).
4. I. Romero, J. Aizpurua, G. W. Bryant, and F. J. García De Abajo, "Plasmons in nearly touching metallic nanoparticles: singular response in the limit of touching dimers," Opt. Express **14**, 9988–9999 (2006).
5. H. Xu, E. J. Bjerneld, M. Käll, and L. Börjesson, "Spectroscopy of single hemoglobin molecules by surface enhanced raman scattering," Phys. Rev. Lett. **83**, 4357 (1999).
6. J. Aizpurua, G. W. Bryant, L. J. Richter, F. G. De Abajo, B. K. Kelley, and T. Mallouk, "Optical properties of coupled metallic nanorods for field-enhanced spectroscopy," Phys. Rev. B **71**, 235420 (2005).
7. S. Kim, J. Jin, Y.-J. Kim, I.-Y. Park, Y. Kim, and S.-W. Kim, "High-harmonic generation by resonant plasmon field enhancement," Nature **453**, 757–760 (2008).
8. I.-Y. Park, S. Kim, J. Choi, D.-H. Lee, Y.-J. Kim, M. F. Kling, M. I. Stockman, and S.-W. Kim, "Plasmonic generation of ultrashort extreme-ultraviolet light pulses," Nat. Photon. **5**, 677–681 (2011).

#290294 https://doi.org/10.1364/OE.25.013760
Journal © 2017 Received 15 Mar 2017; revised 27 Apr 2017; accepted 29 Apr 2017; published 8 Jun 2017

Optics EXPRESS

9. S. Savasta, R. Saija, A. Ridolfo, O. Di Stefano, P. Denti, and F. Borghese, "Nanopolaritons: vacuum rabi splitting with a single quantum dot in the center of a dimer nanoantenna," ACS Nano **4**, 6369–6376 (2010).
10. J. N. Anker, W. P. Hall, O. Lyandres, N. C. Shah, J. Zhao, and R. P. Van Duyne, "Biosensing with plasmonic nanosensors," Nat. Mater. **7**, 442–453 (2008).
11. M. Grzelczak, J. Vermant, E. M. Furst, and L. M. Liz-Marzán, "Directed self-assembly of nanoparticles," ACS Nano **4**, 3591–3605 (2010).
12. T.-C. Lee and O. A. Scherman, "Formation of dynamic aggregates in water by cucurbit [5] uril capped with gold nanoparticles," Chem. Commun. **46**, 2438–2440 (2010).
13. Y. Kang, K. J. Erickson, and T. A. Taton, "Plasmonic nanoparticle chains via a morphological, sphere-to-string transition," J. Am. Chem. Soc. **127**, 13800–13801 (2005).
14. R. Esteban, R. W. Taylor, J. J. Baumberg, and J. Aizpurua, "How chain plasmons govern the optical response in strongly interacting self-assembled metallic clusters of nanoparticles," Langmuir **28**, 8881–8890 (2012).
15. M. Grzelczak, J. Pérez-Juste, P. Mulvaney, and L. M. Liz-Marzán, "Shape control in gold nanoparticle synthesis," Chem. Soc. Rev. **37**, 1783–1791 (2008).
16. R. W. Taylor, R. Esteban, S. Mahajan, J. Aizpurua, and J. J. Baumberg, "Optimizing sers from gold nanoparticle clusters: Addressing the near field by an embedded chain plasmon model," J. Phys. Chem. C **120**, 10512–10522 (2016).
17. A. Alu and N. Engheta, "Theory of linear chains of metamaterial/plasmonic particles as subdiffraction optical nanotransmission lines," Phys. Rev. B **74**, 205436 (2006).
18. A. F. Koenderink and A. Polman, "Complex response and polariton-like dispersion splitting in periodic metal nanoparticle chains," Phys. Rev. B **74**, 033402 (2006).
19. P. Ghenuche, I. Cormack, G. Badenes, P. Loza-Alvarez, and R. Quidant, "Cavity resonances in finite plasmonic chains," Appl. Phys. Lett. **90**, 041109 (2007).
20. N. Harris, M. D. Arnold, M. G. Blaber, and M. J. Ford, "Plasmonic resonances of closely coupled gold nanosphere chains," J. Phys. Chem. C **113**, 2784–2791 (2009).
21. E. Prodan and P. Nordlander, "Plasmon hybridization in spherical nanoparticles," J. Chem. Phys. **120**, 5444–5454 (2004).
22. J. Zuloaga, E. Prodan, and P. Nordlander, "Quantum description of the plasmon resonances of a nanoparticle dimer," Nano Lett. **9**, 887–891 (2009).
23. C. Girard, E. Dujardin, M. Li, and S. Mann, "Theoretical near-field optical properties of branched plasmonic nanoparticle networks," Phys. Rev. Lett. **97**, 100801 (2006).
24. M. I. Stockman, L. N. Pandey, L. S. Muratov, and T. F. George, "Giant fluctuations of local optical fields in fractal clusters," Phys. Rev. Lett. **72**, 2486 (1994).
25. V. M. Shalaev, R. Botet, D. Tsai, J. Kovacs, and M. Moskovits, "Fractals: localization of dipole excitations and giant optical polarizabilities," Physica A **207**, 197–207 (1994).
26. S. J. Barrow, A. M. Funston, D. E. Gómez, T. J. Davis, and P. Mulvaney, "Surface plasmon resonances in strongly coupled gold nanosphere chains from monomer to hexamer," Nano Lett. **11**, 4180–4187 (2011).
27. L. S. Slaughter, B. A. Willingham, W.-S. Chang, M. H. Chester, N. Ogden, and S. Link, "Toward plasmonic polymers," Nano Lett. **12**, 3967–3972 (2012).
28. T. Chen, M. Pourmand, A. Feizpour, B. Cushman, and B. M. Reinhard, "Tailoring plasmon coupling in self-assembled one-dimensional au nanoparticle chains through simultaneous control of size and gap separation," J. Phys. Chem. Lett. **4**, 2147–2152 (2013).
29. Z. Li, S. Butun, and K. Aydin, "Touching gold nanoparticle chain based plasmonic antenna arrays and optical metamaterials," ACS Photonics **1**, 228–234 (2014).
30. D. Citrin, "Plasmon polaritons in finite-length metal-nanoparticle chains: the role of chain length unravelled," Nano Lett. **5**, 985–989 (2005).
31. M. D. Arnold, M. G. Blaber, M. J. Ford, and N. Harris, "Universal scaling of local plasmons in chains of metal spheres," Opt. Express **18**, 7528–7542 (2010).
32. R. W. Taylor, R. Esteban, S. Mahajan, R. Coulston, O. A. Scherman, J. Aizpurua, and J. J. Baumberg, "Simple composite dipole model for the optical modes of strongly-coupled plasmonic nanoparticle aggregates," J. Phys. Chem. C **116**, 25044–25051 (2012).
33. A. M. Smith, M. C. Mancini, and S. Nie, "Bioimaging: second window for in vivo imaging," Nat. Nanotechnol. **4**, 710–711 (2009).
34. M.-F. Tsai, S.-H. G. Chang, F.-Y. Cheng, V. Shanmugam, Y.-S. Cheng, C.-H. Su, and C.-S. Yeh, "Au nanorod design as light-absorber in the first and second biological near-infrared windows for in vivo photothermal therapy," ACS Nano **7**, 5330–5342 (2013).
35. S. T. Jones, R. W. Taylor, R. Esteban, E. K. Abo-Hamed, P. H. Bomans, N. A. Sommerdijk, J. Aizpurua, J. J. Baumberg, and O. A. Scherman, "Gold nanorods with sub-nanometer separation using cucurbit [n] uril for sers applications," Small **10**, 4298–4303 (2014).
36. K. G. Thomas, S. Barazzouk, B. I. Ipe, S. S. Joseph, and P. V. Kamat, "Uniaxial plasmon coupling through longitudinal self-assembly of gold nanorods," J. Phys. Chem. B **108**, 13066–13068 (2004).
37. P. Y. Kim, J.-W. Oh, and J.-M. Nam, "Controlled co-assembly of nanoparticles and polymer into ultralong and continuous one-dimensional nanochains," J. Am. Chem. Soc. **137**, 8030–8033 (2015).

Optics EXPRESS

38. A. Klinkova, H. Thérien-Aubin, A. Ahmed, D. Nykypanchuk, R. M. Choueiri, B. Gagnon, A. Muntyanu, O. Gang, G. C. Walker, and E. Kumacheva, "Structural and optical properties of self-assembled chains of plasmonic nanocubes," Nano Lett. **14**, 6314–6321 (2014).
39. C. J. Murphy, L. B. Thompson, A. M. Alkilany, P. N. Sisco, S. P. Boulos, S. T. Sivapalan, J. A. Yang, D. J. Chernak, and J. Huang, "The many faces of gold nanorods," J. Phys. Chem. Lett. **1**, 2867–2875 (2010).
40. N. Ortiz and S. E. Skrabalak, "On the dual roles of ligands in the synthesis of colloidal metal nanostructures," Langmuir **30**, 6649–6659 (2014).
41. R. Esteban, G. Aguirregabiria, A. G. Borisov, Y. M. Wang, P. Nordlander, G. W. Bryant, and J. Aizpurua, "The morphology of narrow gaps modifies the plasmonic response," ACS Photonics **2**, 295–305 (2015).
42. F. Benz, C. Tserkezis, L. O. Herrmann, B. de Nijs, A. Sanders, D. O. Sigle, L. Pukenas, S. D. Evans, J. Aizpurua, and J. J. Baumberg, "Nanooptics of molecular-shunted plasmonic nanojunctions," Nano Lett. **15**, 669–674 (2014).
43. P. B. Johnson and R.-W. Christy, "Optical constants of the noble metals," Phys. Rev. B **6**, 4370 (1972).
44. T. V. Teperik, P. Nordlander, J. Aizpurua, and A. G. Borisov, "Robust subnanometric plasmon ruler by rescaling of the nonlocal optical response," Phys. Rev. Lett. **110**, 263901 (2013).
45. F. G. De Abajo and J. Aizpurua, "Numerical simulation of electron energy loss near inhomogeneous dielectrics," Phys. Rev. B **56**, 15873 (1997).
46. F. G. de Abajo and A. Howie, "Retarded field calculation of electron energy loss in inhomogeneous dielectrics," Phys. Rev. B **65**, 115418 (2002).
47. A. Alu and N. Engheta, "Tuning the scattering response of optical nanoantennas with nanocircuit loads," Nat. Photon. **2**, 307–310 (2008).
48. L. Novotny, "Effective wavelength scaling for optical antennas," Phys. Rev. Lett. **98**, 266802 (2007).
49. N. Engheta, A. Salandrino, and A. Alù, "Circuit elements at optical frequencies: nanoinductors, nanocapacitors, and nanoresistors," Phys. Rev. Lett. **95**, 095504 (2005).
50. M. Staffaroni, J. Conway, S. Vedantam, J. Tang, and E. Yablonovitch, "Circuit analysis in metal-optics," Phot. Nano. Fund. Appl. **10**, 166–176 (2012).
51. F. Benz, B. De Nijs, C. Tserkezis, R. Chikkaraddy, D. O. Sigle, L. Pukenas, S. D. Evans, J. Aizpurua, and J. J. Baumberg, "Generalized circuit model for coupled plasmonic systems," Opt. Express **23**, 33255–33269 (2015).
52. B. P. Joshi and Q.-H. Wei, "Cavity resonances of metal-dielectric-metal nanoantennas," Opt. Express **16**, 10315–10322 (2008).
53. T. Søndergaard and S. Bozhevolnyi, "Slow-plasmon resonant nanostructures: Scattering and field enhancements," Phys. Rev. B **75**, 073402 (2007).
54. J. Dorfmüller, R. Vogelgesang, R. T. Weitz, C. Rockstuhl, C. Etrich, T. Pertsch, F. Lederer, and K. Kern, "Fabry-pérot resonances in one-dimensional plasmonic nanostructures," Nano Lett. **9**, 2372–2377 (2009).
55. C. Tserkezis, R. Esteban, D. Sigle, J. Mertens, L. Herrmann, J. Baumberg, and J. Aizpurua, "Hybridization of plasmonic antenna and cavity modes: Extreme optics of nanoparticle-on-mirror nanogaps," Phys. Rev. A **92**, 053811 (2015).
56. E. C. Le Ru, W. R. Somerville, and B. Auguié, "Radiative correction in approximate treatments of electromagnetic scattering by point and body scatterers," Phys. Rev. A **87**, 012504 (2013).
57. Z. Wang, B. Luk'yanchuk, W. Guo, S. Edwardson, D. Whitehead, L. Li, Z. Liu, and K. Watkins, "The influences of particle number on hot spots in strongly coupled metal nanoparticles chain," J. Chem. Phys. **128**, 094705 (2008).
58. T. Neuman, C. Huck, J. Vogt, F. Neubrech, R. Hillenbrand, J. Aizpurua, and A. Pucci, "Importance of plasmonic scattering for an optimal enhancement of vibrational absorption in seira with linear metallic antennas," J. Phys. Chem. C **119**, 26652–26662 (2015).
59. Z. Yang, J. Aizpurua, and H. Xu, "Electromagnetic field enhancement in ters configurations," J. Raman Spectrosc. **40**, 1343–1348 (2009).
60. V. Lebedev, S. Vergeles, and P. Vorobev, "Giant enhancement of electric field between two close metallic grains due to plasmonic resonance," Opt. Lett. **35**, 640–642 (2010).
61. S. Lin, M. Li, E. Dujardin, C. Girard, and S. Mann, "One-dimensional plasmon coupling by facile self-assembly of gold nanoparticles into branched chain networks," Adv. Mater. **17**, 2553–2559 (2005).
62. L. S. Slaughter, L.-Y. Wang, B. A. Willingham, J. M. Olson, P. Swanglap, S. Dominguez-Medina, and S. Link, "Plasmonic polymers unraveled through single particle spectroscopy," Nanoscale **6**, 11451–11461 (2014).
63. C. Hanske, M. Tebbe, C. Kuttner, V. Bieber, V. V. Tsukruk, M. Chanana, T. A. König, and A. Fery, "Strongly coupled plasmonic modes on macroscopic areas via template-assisted colloidal self-assembly," Nano Lett. **14**, 6863–6871 (2014).
64. L. Chuntonov, M. Bar-Sadan, L. Houben, and G. Haran, "Correlating electron tomography and plasmon spectroscopy of single noble metal core–shell nanoparticles," Nano Lett. **12**, 145–150 (2011).
65. M. Zhu, P. Chen, W. Ma, B. Lei, and M. Liu, "Template-free synthesis of cube-like ag/agcl nanostructures via a direct-precipitation protocol: highly efficient sunlight-driven plasmonic photocatalysts," ACS Appl.Mater. Interfaces **4**, 6386–6392 (2012).

Optics EXPRESS

1. Introduction

The ability of metallic nanoparticles to capture optical electromagnetic fields thanks to the excitation of localized surface plasmons has attracted much attention during the last years. The plasmonic response of a nanoparticle strongly depends on the material properties, size and shape of the particles as well as on the surrounding medium [1, 2]. Additionally, coupling between particles introduces versatile ways to tune the resonance wavelength as well as to obtain strong near field localization and enhancement in the gap region formed between particles [3, 4]. These strong near fields can be used in a variety of experimental set-ups in optics such as in field-enhanced spectroscopies [5, 6], high harmonic generation [7, 8], strong coupling [9] or sensing of minute amounts of analyte [10] to cite some applications.

Among all the possible plasmonic substrates, self-assembled aggregates composed by small nanoparticles emerge as versatile structures that do not require complex fabrication set-ups [11], with molecular linkers allowing to achieve consistent gap separations down to $\approx$ 1 nm [12]. The particles can self-assemble to form chain-like structures [13] or more complex 3-dimensional aggregates, where the position of each particle is essentially stochastic [12, 14]. Crucially, it is possible to obtain a reproducible overall plasmonic response even for quite complex aggregates, and to control it to a considerable extent by changing the size and shape of the particles and the conditions of aggregation [11, 15]. Nonetheless, engineering the properties of the plasmon resonances remains in general less flexible than for top-down fabrication.

Figure 1(a) sketches a typical situation of self-assembled spherical particles aggregated in the Diffusion-Limited Regime. We consider that a small molecular linker fixes the interparticle distance. The optical response of such an aggregate can be tuned by modifying the self-assembly conditions (particle size, material, linker, concentrations,...). The resulting aggregate presents a branched configuration of particles separated by well defined nanometer gaps [12, 14]. We have argued in previous work [14, 16] that much of the resulting plasmonic response can be understood by modelling the system as an ensemble of chains of adequate lengths (Fig. 1). Thus, understanding the case of straight chains [17, 18] is a critical step to optimize these complex systems, as also to predict the optical response when independent chains are directly synthesized.

Chains of spherical particles interacting across nanometer gaps have received considerable attention [4, 14, 19–25]. The optical response of these chains (blue line in Fig. 1(e)) present a strong dipolar longitudinal chain plasmon (LCP) mode, which redshifts as the number of particles in the chain increases and which is characterized by the generation of very strong and localized near fields in the gap regions, thus making them interesting for spectroscopic studies.

Nonetheless, the redshift of the LCP saturates for chains formed by $\sim$ 10 spherical particles [20, 26–29]. The saturation limits the tunability of the system, making it necessary to use relatively large spheres and very narrow gaps when resonances in the infrared are sought [30–32], as for example when working in the biological window [33, 34]. To increase the tunability, a straightforward possibility is to change the morphology of the particles. However, the results on chains of rods suggest that, as far as the terminations remain spherical, the redshift can be larger than for spheres but the response still saturates with the number of particles [35]. Furthermore, the self-assembly process may become challenging for elongated or very complex particles.

On the other hand, chemically-synthesized particles in self-assembled aggregates present flat facets either by design or due to unavoidable reconfiguration processes inherent to the chemical synthesis [36–38] (see also refs. [39,40] and references therein for a discussion on growth of gold nanoparticles). Thus addressing theoretically the effects that facets have in the plasmonic response of self-assembled aggregates can have direct implications in the interpretation of experimental results. We showed recently very distinct optical behaviour for rod dimers terminated by a flat surface, compared to spherically capped rods [41]. We argue below that such flat facets can be advantageous for applications based on self-assembled systems, notably by improving the tunability of the optical response of the system. Large facets are able to accommodate a larger

Optics EXPRESS

number of molecules in the gap, a situation beneficial for applications that do not require to work at the single molecule level [42]. Figure 1 sketches the main idea for the analysis in this paper in the absence (Figs. 1(a) or 1(b)) or presence (Figs. 1(c) and 1(d)) of faceting in the particle units. Branched aggregates (Figs. 1(a) and 1(c)) are considered to behave as an ensemble of non-interacting straight chains (Figs. 1(b) and 1(d)), an approach substantiated by a previous study using experimental particles that showed how chain calculations can be enough to nicely and effectively reproduce the optical response of the full aggregate [14]. For linearly polarized light, the polarization of the external field selects the excitation of chain modes parallel to the incident field (Figs. 1(a) and 1(c)). On the other hand, if unpolarized light is used, plasmonic modes can be efficiently excited in all chains that are oriented in any direction perpendicular to the propagation direction of the excitation beam.

The faceting at each particle unit within a straight chain strongly affects the optical response (Fig. 1(e)). For the same number and size of particles, the resulting resonances are found at larger wavelengths for chains of particles with large facets than for chains of spheres (red line for flat-faceted particles chain vs. blue line for spheres in Fig. 1(e)). In the following theoretical work, we analyze in a systematic way the behaviour of chains of different length and facet size. In particular, we focus on the influence of the size of the facets on the tunability and the field enhancement in the gap regions, with direct implications for spectroscopy and sensing at infrared frequencies.

2. Model

We simulate 1-dimensional chains (Figs. 1(b) and 1(d)) composed by cylindrical gold nanoparticles described by the experimental permittivity of gold [43] and surrounded by vacuum. For simplicity, the full structure is rotationally symmetric, even if the more complex 3-dimensional aggregates with flat facets in Fig. 1c would require less symmetrical particles. The length of the particles along the chain axis is $L = 50$ nm, their diameter along the orthogonal plane is also $D = 50$ nm and the separation in the gaps is $d_{gap} = 1$ nm. The rods are capped by a flat surface of diameter D_f, with the radius of the rounded edge $r_{edge} = \frac{D-D_f}{2}$ (see zoom of Fig. 1(d)). We vary the diameter of these gap facets from $D_f = 0$ nm to $D_f = 46$ nm, where the former corresponds to the limit situation of a sphere of diameter $D = 50$ nm (zoom in Fig. 1(b)). Plane wave illumination at wavelength λ with the electric field of amplitude E polarized along the chain axis is used to excite the strong longitudinal plasmonic resonance of the system. We then analyze the optical response of the plasmonic chains in the far-field and in the near-field as a function of the number of particles in the chain (N_p) and the facet diameter (D_f). The gap distance ($d_{gap} = 1$ nm) is short enough that non-local effects would introduce some modification in the exact resonance frequency and strength of the plasmonic modes, however previous studies have shown that considering non-locality in calculations of gold systems is equivalent to assuming a slightly shifted surface interface inside the metal by about 0.9 to 1.5 Å [44]. This effective displacement of the interfaces creates an effective gap distance which is about 1.7-3 Å larger than in the local treatment. To simplify the discussion of the properties of the chain modes and focus on the dependence on the morphology, we develop all our study within the local description.

To analyze the near-field properties in the gaps, we calculate the near-field enhancement in the central plane of all gaps, for a region corresponding to a circle of 25 nm of radius centred in the chain axis (area inside the dashed circle in the zoom of Figs. 1(b) and 1(d)). We then evaluate two different quantities. On the one hand we study the maximum near-field enhancement, $|E/E_0|_{max}$, which corresponds to the maximum field enhancement produced in the gaps. On the other hand we consider the average field enhancement, $|E/E_0|_{avr}$, by averaging the near-fields calculated in all the gaps of a particular chain. We use the Boundary Element Method (BEM) [45, 46] optimized for cylindrically symmetric systems to solve the Maxwell's equations. BEM is a surface method, and thus only the boundary conditions at the surfaces need to be considered for

Optics EXPRESS

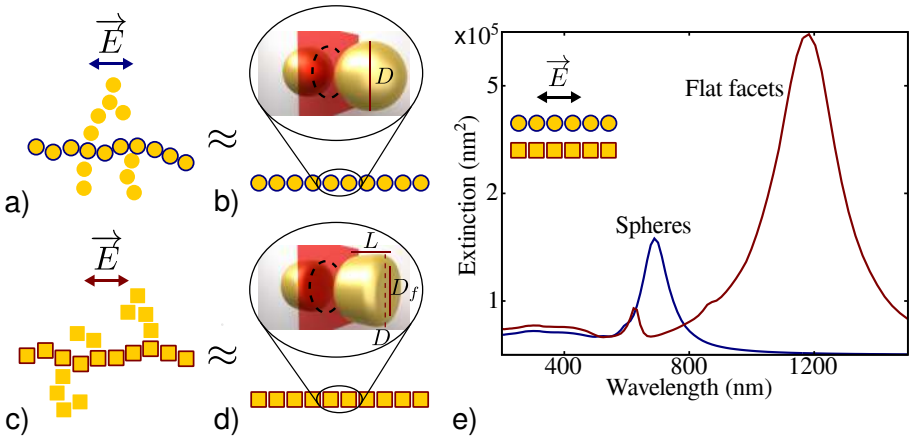

Fig. 1. Scheme of aggregates of a) spheres and c) flat-faceted particles under plain wave illumination with electric field $\vec{E}$. The incoming illumination mainly excites longitudinal plasmon modes in chains that extend along the polarization direction (chains delimited in the scheme by thick blue or red lines). We thus focus on the optical response of chains of b) spheres or d) flat-faceted particles. Zooms in b) and d) illustrate the dimensions of the particles composing the chains. In both cases the particles are rotationally symmetric with respect to the chain axis. We notice that the complex flat-faceted aggregates in c) would require breaking the rotational symmetry to have more than 2 flat facets per particle. The spheres (b) are defined by their diameter $D = 50$ nm. The flat-faceted particles (d) are rods defined by 3 parameters, the length L (in the direction along the chain axis), the diameter D (in the orthogonal direction) and the facet diameter D_f. $r_{edge} = \frac{D-D_f}{2}$ is the radius of the edges of the particles. We fix $L = D = 50$ nm and we vary D_f from $D_f = 0$ nm, corresponding to a sphere, to $D_f = 46$ nm, a cylindrical rod with almost completely flat facets. In Figs. 4–6 the fields are evaluated in the central plane of the gaps, in an area corresponding to a circle of radius 25 nm. We mark this region for one gap in the insets of b) and d) as the region of the central red plane delimited by the dashed circular line. e) Calculated extinction spectrum of a chain of $N_p = 10$ spheres in blue and a chain of 10 flat-faceted particles with $D_f = 46$ nm in red for incident light with the electric field polarized along the chain direction. All the structures considered in this study are cylindrically symmetric.

solving the optical response (the Maxwell's equations in the medium are automatically verified).

3. Far-field response

In order to show the strong impact that the faceting has in the optical response of the chains, Fig. 1(e)) shows the extinction cross section of chains formed by $N_p = 10$ particles composed by spheres (blue) and by $D_f = 46$ nm flat-faceted particles (red). The presence of the flat facets strongly influences the spectral position of the lowest-energy plasmon resonance by shifting it to longer wavelengths.

For a more detailed analysis of the far-field response of the system, Fig. 2 shows the normalized extinction cross-section for chains of different length, both considering spherical particles ($D_f = 0$ nm, Fig. 2(a)) as well as particles with the largest flat termination considered ($D_f = 46$ nm, Fig. 2(b)). All the spectra show a dominant plasmonic peak ($\lambda > 500$ nm) associated with the lowest-energy longitudinal chain plasmon (LCP) of dipolar character, which redshifts as the number of particles increases. For spherical particles (Fig. 2(a)) the shift saturates for chains with $N_p \sim 10$ particles, showing a maximum shift with respect to the resonance of a single

Optics EXPRESS

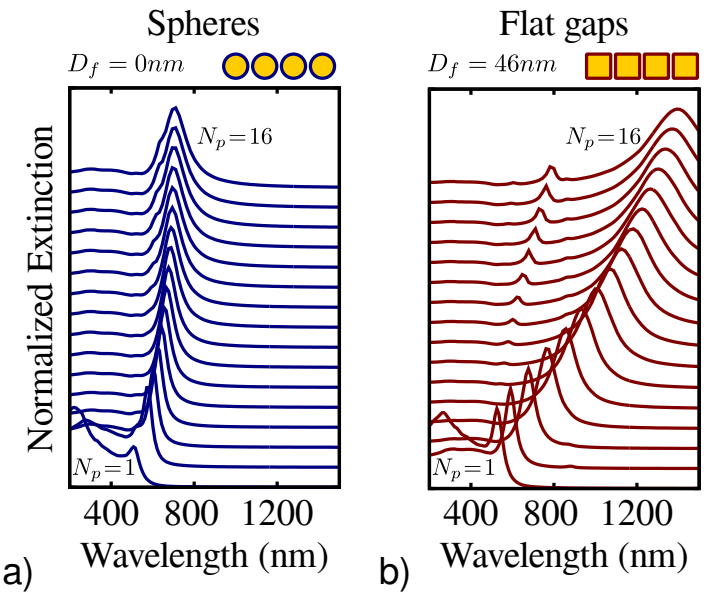

Fig. 2. a),b) Waterfall plot of the normalized extinction cross-section calculated as a function of wavelength for a chain of Au particles for a) D_f = 0 nm (spheres) and b) rods with D_f = 46 nm facets for increasing number of particles N_p = 1 − 16. Shorter chains are plotted at the bottom. All the structures considered in this study are cylindrically symmetric, and the different spectra are shifted vertically for clarity.

sphere that is relatively small [20, 26–29]. In contrast, in the case of flat-terminated particles (Fig. 2(b)) the saturation of the redshift is less pronounced even for chains formed by up to $N_p \sim 16$ particles and the resonance wavelength of the LCP continues to increase with chain length. It is thus possible to tune the response of flat-faceted particles over a much larger spectral range than for spherical ones. Additionally, for flat-gap chains formed by $N_p \gtrsim 10$ particles, a higher order longitudinal mode that redshifts with increasing N_p is also excited at lower wavelengths ($\lambda \approx 625$ nm).

Further insight into the strong influence of the gap morphology on the optical response can be obtained by observing the evolution of the lowest-energy longitudinal chain plasmon resonance (λ_{LCP}) with increasing number of particles in the chain, N_p (Fig. 3(a), dots) and for different sizes of the gap facet (D_f = 46 nm, 34 nm, 24 nm, 14 nm, 0 nm top to bottom). For comparison, Fig. 3(a) also shows the dipolar plasmon resonance of a rod of 50 nm diameter and increasing length, capped by flat terminations with D_f = 46 nm. The resonant shift of the LCP for small chains is similar for all the facet morphologies. However, D_f strongly affects how λ_{LCP} evolves as the chain gets longer. The shift for the chain of spheres deviates from the general trend for very small number of particles in the chain ($N_p \approx 3$), saturating for a smaller N_p, and thus the maximum shift with respect to the single particle resonance wavelength $\lambda_{SP} \approx 510$ nm remains comparatively small ($\lambda_{LCP} - \lambda_{SP} \approx 200$ nm, bottom line in Fig. 3(a)). As the facet size increases, the shift of the dipolar LCP reaches saturation for longer chains (upper lines in Fig. 3(a)) so that larger shifts are possible. In the case of D_f = 46 nm we obtain $\lambda_{LCP} - \lambda_{SP} \approx 800$ nm for N_p = 16, a length still far from saturation. This behaviour can be connected with the response of a rod dimer with flat gap terminations [41], where the narrow flat gap is seen as a capacitor [47] whose capacitance becomes larger as the gap closes and eventually behaves as a short-circuit. Thus, the chains for D_f = 46 nm and very narrow gaps approach the behaviour of a single "connected" rod of the same length, characterized by strong, and approximately linear,

Optics EXPRESS

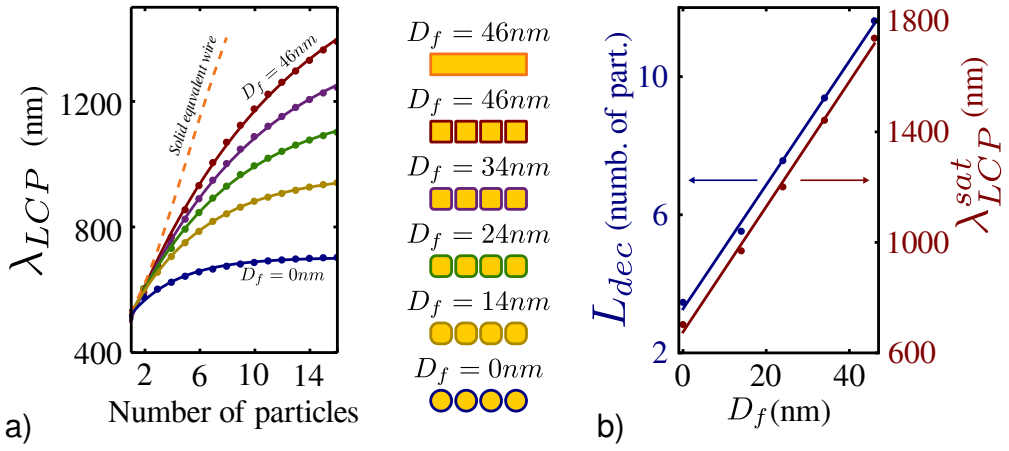

Fig. 3. a) Spectral position of the lowest-energy longitudinal chain plasmon (λ_{LCP}) calculated as a function of the number of particles in the chain N_p, for different diameters D_f of the flat facet forming the gaps (top to bottom, D_f =46 nm, 34 nm, 24 nm, 14 nm, 0 nm). The different colours in the plot indicate the corresponding structure in the central panel (recall that the particles are cylindrically symmetric). The calculated values (dots) are fitted to an exponential function (solid lines). We also show the results for a rod of length $N_p \cdot L$ (an orange dashed line). c) Parameters of the exponential fit for each facet diameter corresponding to the saturation wavelength λ^{sat}_{LCP} (red, right axis) and the decay length L_{dec} (blue, left axis). Dots are the calculated values while lines are a linear fit.

shifts [6,48] (orange dashed line in Fig. 3(a)). We have verified that the similarity between the single rod and the D_f = 46 nm chain increases if the gap distance is decreased.

The redshift follows quite closely an exponential dependence with N_p for all facets considered, which generalizes the tendencies observed in previous work for spheres [20]. The solid lines in Fig. 3(a) correspond to a fit of the calculated data (dots) using the function

$$\lambda_{LCP} = \lambda^{sat}_{LCP} - \beta e^{-N_p/L_{dec}} \tag{1}$$

where λ^{sat}_{LCP} is the saturation wavelength of the longitudinal chain plasmon and L_{dec} is the decay length (measured in number of particles). The fit is very satisfactory in all cases.

In Fig. 3(b) we analyze the fitting parameters obtained from the calculations in Fig. 3(a) as a function of the facet diameter D_f. The red dots (right axis) show how the saturation wavelength λ^{sat}_{LCP} increases for larger facet size, going from λ^{sat}_{LCP} = 705 nm for spheres, to λ^{sat}_{LCP} = 1760 nm for D_f = 46 nm particles. The redshift with respect to the single particle resonance ($\lambda^{sat}_{LCP} - \lambda_{SP}$) is thus a factor of ∼ 6 larger for the large flat facets than for spheres. A similar behaviour is observed for the decay length L_{dec} (blue dots and left axis in Fig. 3(b)), which increases monotonously from L_{dec} = 3.5 particles for spheres to L_{dec} = 11.8 particles for D_f = 46 nm flat-faceted particles. Interestingly, the evolution of both λ^{sat}_{LCP} and L_{dec} with N_p can be fitted very satisfactorily by a simple linear function (solid lines in Fig. 3(b)), which makes it straightforward to determine the particular flatness D_f and particle number N_p to obtain a resonance at a desired energy.

To understand the linear dependence of λ^{sat}_{LCP} with D_f we consider an infinite chain, ignoring losses. Each unit cell of the resulting periodic structure can be modelled as a inductance $\mathbb{L}$ characterizing the metallic particle and a capacitance C associated to the inter-particle gaps, leading to a total impedance $Z = i\mathbb{L}\omega + \frac{1}{i\omega C}$ where ω is the (angular) frequency and i is the imaginary unit [49–51]. The resonant frequency thus corresponds to $\omega^{\infty}_{res} = \frac{1}{\sqrt{\mathbb{L}C}}$. Using the

capacitance of two parallel plates of area A separated by the gap distance d_{gap}, $C = \frac{\epsilon A}{d_{gap}}$, where ϵ is the dielectric constant of the material between the plates, and substituting A by the facet area, we get $\omega_{res}^{\infty} = \left(\mathbb{L}\epsilon\pi(D_f/2)^2/d_{gap}\right)^{-1/2} \propto 1/D_f$. Therefore, $\lambda_{LCP}^{sat} = \lambda_{res}^{\infty} \propto 1/\omega_{res}^{\infty} \propto D_f$ reproducing the linear proportionality with D_f found in Fig. 3(b). This simple model thus exhibits the trends found for λ_{LCP}^{sat}. Nonetheless, a full understanding would require more complex models. For example, this simple equation wrongly predicts $\lambda_{LCP}^{sat} \to 0$ for $D_f \to 0$, which may be the consequence of neglecting the intrinsic capacitance of the metallic particles and the contribution to the gap capacitance of the region outside the flat facets.

4. Near-field response

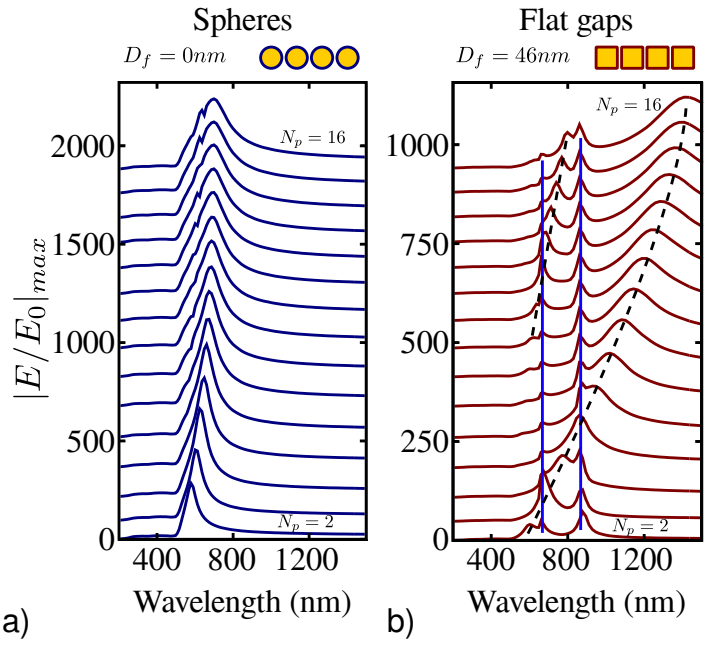

Fig. 4. a),b) Waterfall plot of the maximum near-field enhancement at the gaps of a chain of Au particles with a) $D_f = 0$ nm and b) $D_f = 46$ nm facets calculated as a function of wavelength and number of particles $N_p = 2-16$. Shorter chains are plotted at the bottom. In b) black dashed lines track the position of the LCP resonances while blue lines correspond to the position of the $TCPs$. All the structures considered in this study are cylindrically symmetric, and the different spectra are shifted vertically for clarity.

We analyze next the evolution of the maximum near-field enhancement $|E/E_0|_{max}$ at the gaps with N_p, obtained by evaluating the fields in the middle plane of the gaps as described in section 2, both for spherical particles (Fig. 4(a)) and for flat-terminated particles with $D_f = 46$ nm (Fig. 4(b)). For spherical particles we observe the same predominant lowerst-energy LCP mode found in the far-field response, which redshifts with increasing N_p until it saturates. $|E/E_0|_{max}$ reaches values of the order of several hundreds for this resonance. For large N_p, we also observe a small narrow peak at a lower wavelength than the main maxima, which would correspond to a higher order LCP. In contrast, chains formed by flat-faceted particles support two distinct sets of modes, revealing the existence of non-radiative modes that were not present in the far-field spectrum [41,52]. First, we can readily identify the strongly radiant LCP modes on the near-field response (black dashed lines) because their spectral evolution is known from the analysis of the extinction peaks in Fig. 2(b). On the other hand, a new set of modes emerges on the field

Optics EXPRESS

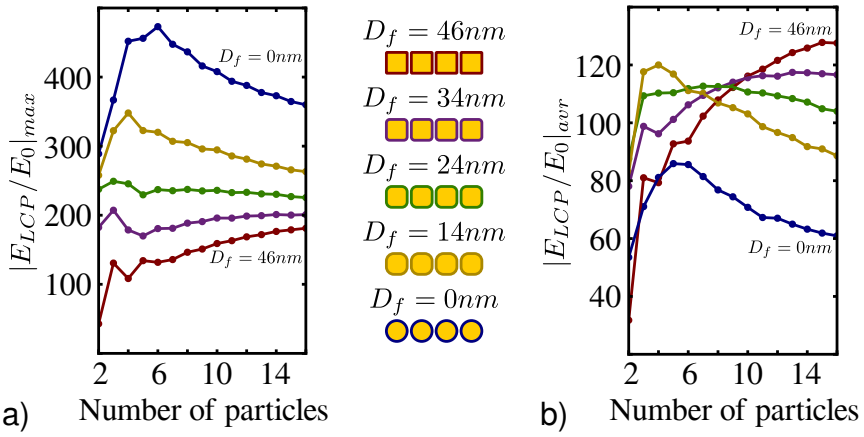

Fig. 5. a) Maximum near-field enhancement $|E_{LCP}/E_0|_{max}$ of the lowest-energy longitudinal chain plasmon (LCP) calculated as a function of the number of particles in the chain N_p, for different diameters D_f (bottom to top , D_f = 46nm, 34nm, 24nm, 14nm, 0nm). b) Average near-field enhancement $|E_{LCP}/E_0|_{avr}$ of the lowest-energy longitudinal chain plasmon (LCP) as a function of the number of particles in the chain N_p, for the same diameters D_f as in Fig. 3. The different colours in the plot indicate the structure under study, as given by the schematics in the central panel of the figure. All particles are cylindrically symmetric.

enhancement spectra, as revealed by the maximum at wavelengths $\lambda \approx 650$ nm and $\lambda \approx 850$ nm (blue vertical lines). The resonant energy of these modes is not significantly affected by changing the length of the chain and, consistently with previous work, we identify them as transverse cavity plasmons $TCPs$, i.e. Fabry-Perot like cavity modes at the gap that appear at energies strongly dependent on the facet diameter [52–54]. The resonant position of the $LCPs$ and the $TCPs$ at the gap behave essentially independently, as marked in Fig. 4(b) with the blue and black dashed lines, i.e. they do not show any clear sign of avoided crossing [41], although mode hybridization can be achieved for other morphologies [55]. When the two modes are simultaneously excited (spectral match), the enhancement produced by both of the resonances lead to larger enhancement values.

For a more direct comparison of the effects of the morphology on the maximum field enhancement, Fig. 5(a) shows $|E/E_0|_{max}$ at the wavelength of the dipolar (lowest-energy) LCP peak ($|E_{LCP}/E_0|_{max}$) as a function of N_p, for the same values of D_f considered earlier. As could be expected, chains of spheres lead to the strongest enhancements of $|E_{LCP}/E_0|_{max} \approx 470$, which is found for chains of 6 spheres. Nevertheless, for $N_p \gtrsim 6$ spheres, $|E_{LCP}/E_0|_{max}$ starts to drop off due to the emergence of significant radiative losses [16, 56, 57]. Particles with small facets follow the same trends as the spherical ones but the local fields are weaker, $|E_{LCP}/E_0|_{max} \approx 345$ for $N_p = 4$ and $D_f = 14$ nm. Finally, short particle chains with larger flat facets exhibit comparatively small $|E_{LCP}/E_0|_{max}$, with some oscillations with increasing N_p, due to the crossing of the LCP and the $TCPs$. Afterwards the maximum enhancement increases continuously reaching $|E_{LCP}/E_0|_{max} \approx 180$ for the largest facets and longest chains.

Although chains of spheres produce larger maximum near-fields than flat-faceted particles, the enhancement remains of the same order of magnitude. Furthermore, for specific applications in spectroscopy and sensing, it is convenient to enhance the field over large areas. Notably, while studies of single molecules placed at the optimal location are sensitive to the maximum near field, large average fields are interesting for applications where a considerable number of molecules are sensed or characterized simultaneously, or when the position of the molecules is not well

controlled. Figure 5(b) shows the average field enhancement in the gaps for the LCP mode, $|E_{LCP}/E_0|_{avr}$, as a function of the number of particles and D_f. The average is calculated as described in section 2. For $N_p \lesssim 5$, $|E_{LCP}/E_0|_{avr}$ generally grows as the chain gets longer. The largest average enhancement is produced for particles with $D_f = 14$ nm, whereas spheres and particles with $D_f = 46$ nm generate the weakest average fields for these short chains. For long chains of spherical particles and particles with $D_f = 14$ nm, $|E_{LCP}/E_0|_{avr}$ again diminishes as N_p grows. In contrast, for particles with large facets ($D_f = 46$ nm and $D_f = 34$ nm) $|E_{LCP}/E_0|_{avr}$ keeps growing significantly with increasing length up to $N_p \approx 14 - 16$.

As a consequence, spherical particles are found not to be optimal to maximize the average field enhancement. To that end, particles with small but non-zero D_f are preferred in short chains, and so are particles with large facets in the case of long chains. We emphasize that, although the dependence of the results in Fig. 5(b) on the chain length and on the facet diameter are relatively complex, strong average fields can be obtained for all types of particle terminations.

We last notice that, depending on the experiment, it may be convenient to average over $|E/E_0|^2$ (for example for infrared absorption [58]) or over $|E/E_0|^4$ (for Raman spectroscopy [59]). We thus analyze the averages of $|E_{LCP}/E_0|^2$ and $|E_{LCP}/E_0|^4$, calculated similarly to $|E_{LCP}/E_0|_{avr}$ (graph not shown). In the case of $[(|E_{LCP}/E_0|^2)_{avr}]^{1/2}$, short chains of faceted particles with small facets ($D_f = 14$ nm) produce the largest values. For long chains ($N_p = 16$ particles), all the faceted particles with $D_f \geq 14$ nm lead to similar $[(|E_{LCP}/E_0|^2)_{avr}]^{1/2}$. The results for $[(|E_{LCP}/E_0|^4)_{avr}]^{1/4}$ are similar to those in Fig. 5(b) except that $D_f = 14$ nm is optimal for a number of particles of $N_p = 2 - 3$. Notably, long chains characterized by large flat facets always result in large average fields independently of how these fields are averaged.

5. Field localization

In any plasmonic structure it is important to understand how the distribution of field enhancements associated to a plasmonic resonance around the structure is related with the actual localization of the incident light. To that end, we analyze the field distribution near the gaps of the different structures studied in the previous sections. In Figs. 6(a)–6(e) we plot the field enhancement $|E/E_0|$ in the central gap of a $N_p = 8$ particle chain for the dipolar LCP and each facet diameter studied. Particles with flat facets exhibit less intense near fields but distributed over a larger flat area in contrast with the stronger localization and more intense fields of the gaps formed by spherical particles, which agrees with the results of Fig. 5(a). The analysis of the field localization can be made more quantitative by using the normalized mode area $\mathscr{A}_N$,

$$\mathscr{A}_N = \frac{1}{\pi(D/2)^2} \int_S \frac{|E(\vec{r})|^2}{|E^{max}|^2} dS \tag{2}$$

where $|E(\vec{r})|^2$ is the square modulus of the induced field at position $\vec{r}$ in the central plain of the gap, $|E^{max}|^2$ is the maximum of $|E(\vec{r})|^2$, and we normalize by the particles geometrical cross-section $\pi(D/2)^2$. The integral extends over the same 25 nm radius region as described in section 2. We have verified that integrating over a circle of 50 nm radius does not significantly affect the results.

$\mathscr{A}_N$ gives a measure of the confinement of the near-fields in the gap. A value of $\mathscr{A}_N = 0$ would mean that the field is localized at a single point whereas a value $\mathscr{A}_N = 1$ is obtained when the near-field is uniform across the particle cross-section and zero outside. Figure 6(f) shows that $\mathscr{A}_N$ monotonously increases as the facet diameter D_f gets larger (red), evolving from $\mathscr{A}_N = 0.024$ for spheres to $\mathscr{A}_N = 0.83$ for the larger D_f. Two approximations are useful to understand these results. According to previous quasi-static work [60] the near-field between two spherical nanoparticles of diameter D separated by a gap d_{gap} is confined to a circle of radius $\approx \sqrt{(D/2)d_{gap}}$, giving $\mathscr{A}_N \approx 2d_{gap}/D$ (to be compared to the value $\mathscr{A}_N = 1.2d_{gap}/D$ given by the calculations). In the case of large facets, Figs. 6(a)–6(c) indicate that the near-field is

Optics EXPRESS

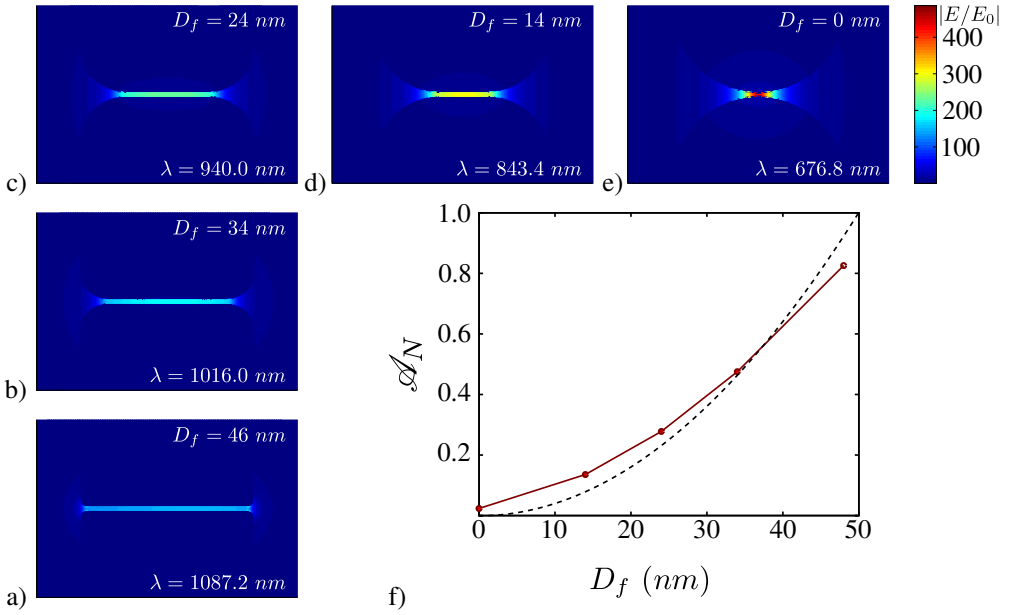

Fig. 6. Near-field maps of the LCP mode calculated near the central gap of a chain formed by $N_p = 8$ particles with faceted diameter a) $D_f = 46$ nm, b) $D_f = 34$ nm, c) $D_f = 24$ nm, d) $D_f = 14$ nm and e) $D_f = 0$ nm. f) The dots and solid line show the LCP normalized mode area $\mathscr{A}_N$ as a function of facet diameter D_f. The dashed line indicate the normalized area D_f^2/D^2 for each structure considered. All the structures considered in this study are cylindrically symmetric.

approximately homogeneous at the gap region between the flat facets and much weaker outside. This would correspond to $\mathscr{A}_N = D_f^2/D^2$, which is represented in Fig. 6(f) by the black dashed line. As we can see, the agreement between the normalized area obtained with this simple expression and that obtained from the calculation is good for intermediate and large facets.

6. Discussion and conclusions

Our analysis has shown that the exact facet morphology plays a key role in determining the optical response of plasmonic chains of particles separated by nanometric gaps, as those that can be obtained by self-assembly. We argue that these results might have direct consequences in more complex branched aggregates [14, 61], whose optical response can be dominated by plasmonic modes supported by chain-like subunits.The description of the optical response of aggregates as ensembles of linear chains is based on the validation of this concept for spherical particles, and we expect it to be valid also in clusters formed by flat-faceted units, at least if the different gaps are always formed between well-aligned flat facets. Furthermore, although the inherent disorder found in self-assembled aggregates modifies to some extent the plasmonic modes, the overall properties of the plasmonic response have been found to be quite robust with respect to disorder in previous work [14, 32, 62, 63]. The experimental realization of such 2 or 3-dimensional aggregates would require particles with more than two flat facets. Multiple facets often occur naturally when trying to synthesize spherical particles [64], and it appears possible to modify the synthesis process to optimize the level of faceting for a given application. Notably, cubes have already been synthesized [65].

The key result of this paper is the much larger tunability of the longitudinal chain plasmon

(LCP) when using flat-capped cylindrical particles than when using spherical ones. Notably, all the geometries studied in this paper exhibit a exponential redshift of the LCP as the chain gets longer, with the decay length L_{dec} and the saturation wavelength λ_{LCP}^{sat} increasing linearly as the facets become larger. In particular, the resonant energy for the case of flat-capped cylindrical particles extends from $\lambda_{SP} \approx 525$ nm for a single particle to a saturation wavelength (as defined in Eq.1) $\lambda_{LCP}^{sat} \approx 1760$ nm, which covers the whole near-infrared biological window [33, 34] and the corresponding decay length is $L_{dec} = 11.8$ particles. In comparison, $\lambda_{LCP}^{sat} \approx 705$ nm and $L_{dec} = 3.4$ particles for spherical particles. Chains of flat-faceted particles are thus a promising alternative in field enhanced spectroscopy and sensing, compared to other self-assembled structures such as chains of rods [35].

Last, we found that flat-faceted particles exhibit near-field enhancements of the same order of magnitude as spheres but distributed over a larger area at the gaps. This larger region of strong enhancement can be used to accommodate more molecules and to facilitate the location of the molecules for field-enhanced spectroscopies, as well as to induce coupling between molecules to boost coherent interactions for quantum information applications. Chains of flat-faceted particles thus seem suitable for experiments requiring optical tunability over a wide spectral range without losing the strong near-field enhancements characteristic of chains of spherical particles.

Funding Information

Spanish Ministry of Economy, Industry and Competitiveness (FIS2016-80174-P); Basque Government (ELKARTEK MICRO4FA); Gipuzkoako Foru Aldundia (European Union Feder funds "Una manera de hacer Europa").